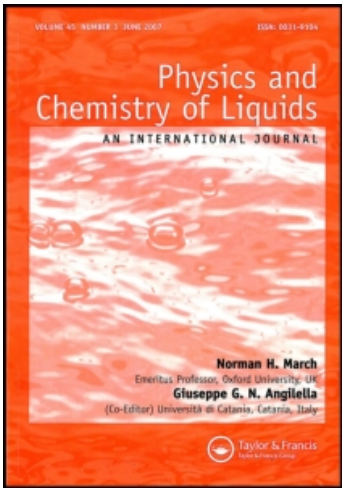

Physics and Chemistry of Liquids
Publication details, including instructions for authors and subscription information:
http://www.informaworld.com/smpp/title~content=t713646857

Structure and Density of Gold-Cesium-Melts. II. Neutron Diffraction with Molten Gold-Cesium-alloys

W. Martin[a]; W. Freyland[ab]; P. Lamparter[a]; S. Steeb[a]
[a] Max-Planck-Institut für Metallforschung Institut für Werkstoffwissenschaften, Stuttgart, West Germany [b] Institut für physikalische Chemie der Universität, Marburg

To cite this Article Martin, W. , Freyland, W. , Lamparter, P. and Steeb, S.(1980) 'Structure and Density of Gold-Cesium-Melts. II. Neutron Diffraction with Molten Gold-Cesium-alloys', Physics and Chemistry of Liquids, 10: 1, 61 — 76
To link to this Article: DOI: 10.1080/00319108008078457
URL: http://dx.doi.org/10.1080/00319108008078457

Phys. Chem. Liq., 1980, Vol. 10, pp. 61-76
0031-9104/80/1001-0061$06.50/0

Structure and Density of Gold-Cesium-Melts

II. Neutron Diffraction with Molten Gold-Cesium-alloys

W. MARTIN, W. FREYLAND†, P. LAMPARTER, and S. STEEB

Max-Planck-Institut für Metallforschung, Institut für Werkstoffwissenschaften, Stuttgart, West Germany.

(*Received February 18, 1980*)

INTRODUCTION

Recently with Au-Cs-melts measurements of some physical properties were done such as electrical conductivity,[1] thermoelectric power,[1] electromigration,[2] and magnetic susceptibility.[3] According to these results appreciable changes in binding must occur during the transition from the pure metal melts to the AuCs-melt. It was assumed that the AuCs-melt is ionic, i.e. consists of Cs^+- and Au^--ions.[4] The difference in Paulings's electronegativities[5] of Cs and Au supported this assumption. This fact led us to the investigation of the structure and the density of Au-Cs-melts.

In the present second part the diffraction experiments performed with fast neutrons on Au-Cs-melts will be presented.

THEORETICAL BACKGROUND

From the differential cross section per atom $(1/N)/d\sigma/d\Omega|_{coh}$ for coherent neutron diffraction the Faber–Ziman total structure factor $S(q)$[6] follows according to Eq. (1):

$$S(q) = \frac{(1/N)\,d\sigma/d\Omega|_{coh} - (\langle b^2\rangle - \langle b\rangle^2)}{\langle b\rangle^2}$$

† Institut für physikalische Chemie der Universität Marburg.

with

N = number of irradiated atoms
$q = 4\pi(\sin\theta)/\lambda$
2θ = scattering angle
λ = wavelength
$\langle b^2\rangle = c_1 b_1^2 + c_2 b_2^2$
$\langle b\rangle = c_1 b_1 + c_2 b_2$
$\langle b^2\rangle - \langle b\rangle^2 = c_1 c_2 (b_1 - b_2)^2$ = monotonic Laue scattering
c_1, c_2 = atomic fractions of element 1, 2
b_1, b_2 = coherent scattering length of element 1, 2

The total pair correlation function $g(r) = \rho(r)/\rho_0$ can be calculated from the total structure factor by Fourier transform according to Eq. (2):

$$g(r) = 1 + \frac{1}{2\pi^2 \rho_0 r} \int_0^\infty q(S(q) - 1)\sin qr \, dq \tag{2}$$

with

$\rho(r)$ = local number density in the distance r from a reference atom
ρ_0 = mean number density

From $g(r)$ we obtain the radial distribution function RDF(r) according to Eq. (3):

$$\mathrm{RDF}(r) = 4\pi r^2 \rho_0 g(r) \tag{3}$$

The distance r^I of nearest neighbours is given by the position of the main maximum of the pair correlation function $g(r)$. The experimental coordination number N^I is obtained from the area below the first maximum of the RDF. For the discussion of short range order phenomena in molten binaries the Bhatia–Thornton partial structure factor S_{NN}, S_{CC}, and S_{NC} are of special interest. S_{NN} means the contribution of number density fluctuations, S_{CC} the contribution of concentration fluctuations, and S_{NC} the contribution of the correlation of density—with concentration fluctuations.

A link between the total structure factor $S(q)$ according to Faber–Ziman and the partial structure factors according to Bhatia and Thornton is given by Eq. (4):

$$S(q) = \left[\langle b\rangle^2 S_{NN} + c_1 c_2 (b_1 - b_2)^2 \left[\frac{S_{CC}}{c_1 c_2} - 1\right] + 2\langle b\rangle (b_1 - b_2) S_{NC}\right] \frac{1}{\langle b\rangle^2} \tag{4}$$

CORRECTION PROCEDURE AND NORMALIZATION

To obtain the total intensity I_{corr} scattered by the specimen alone, the total measured intensity must be corrected for furnace- and container-scattering as well as for selfabsorption in the specimen and absorption in the container. The method is similar to that in Ref. 8 but the total scattering cross section σ_t and the atomic weight M are now mean values weighted according to the atomic concentrations.

The structure factor $S(0)$ needed for the normalization procedure as described in Ref. 8 is unknown in the case of Au-Cs-melts. Therefore this procedure is replaced by the so called vanadium-calibration. This calibration method yields a normalization constant β for the transformation of cross sections given in absolute units into measured pulse rates I. The calculated sum of the incoherent scattering-, the multiple scattering-, and the monotonic Laue scattering-cross sections yields after normalization with β the monotonic contribution to the corrected intensity I_{corr}, which we call background scattering I_b.

$$I_b = \beta \cdot N^s \left[\frac{1}{4\pi} \sigma_{inc} + \frac{1}{4\pi} \sigma_{ms} + \langle b^2 \rangle - \langle b \rangle^2 \right] \tag{5}$$

with

σ_{inc} = incoherent scattering cross section of the alloy
σ_{ms} = cross section for multiple scattering

σ_{ms} is calculated as described in Ref. 9. The ratio of single to double scattering needed is tabulated in Ref. 10. N^s means the number of those atoms in the specimen which are irradiated by the neutron beam. The normalization constant β is determined from the intensity scattered in the q-region from 3.5 $Å^{-1}$ to 11 $Å^{-1}$ by a vanadium-standard with the same dimensions as the specimen to be investigated. For this reference-measurement neither furnace nor container was used, thus the intensity had to be corrected only for self-absorption. Analogous to Eq. (5) we obtain for I_V:

$$I_V = \beta N^V \left[\frac{1}{4\pi} \sigma_{inc}^V + \frac{1}{4\pi} \sigma_{ms}^V \right] \tag{6}$$

Equations (5) and (6) yield I_b from which the total structure factor $S(q)$ can be calculated according to Ref. 8. Equation (7), which is valid for $q \to \infty$ yields a possibility to check the vanadium-calibration:

$$\frac{(I_{corr}(\infty) - I_b)}{(\beta N^s)} = \langle b \rangle^2 \tag{7}$$

The value of $\langle b \rangle^2$ calculated according to Eq. (7) deviates for all specimens by less than $\pm 3\%$ compared to the corresponding value calculated with the

tabulated scattering lengths. Also this check yields the proof for the correctness of $\sigma_{inc}^{Cs} = 0.22$ barn which was evaluated in Ref. 8 and which enters into the present calculation by Eq. (5).

EXPERIMENTAL BACKGROUND AND RESULTS

The neutron diffraction experiments were done as described in Ref. 8. The Au-Cs-melts were contained in electron beam welded cylinders (7 mm diameter; 0.1 mm wall thickness) made from Vanadium-foil. The cylinders were filled within a glovebox in Argon-atmosphere. The sealed containers were annealed at 600°C/8 h. The investigations had to be restricted to the concentration range between zero and 50 at% Au, since it was not possible to obtain homogeneous specimens with larger Au-content. (An annealing treatment at 640°C/24 h with an alloy containing 55 at% Au was unsuccessful, for example.) It should be mentioned that during the present investigations large deviations from the phase diagram reported in Ref. 11 could be found between 10 and 50 at% Au. For example, an alloy containing 25 at% Au showed crystalline reflexes at temperatures up to 90°C above the melting point given in Ref. 11.

The concentrations of the molten alloys were 50, 53, 55, 60, 70, 75, and 80 at% Cs, the temperatures were just 10 to 50°C above the corresponding melting temperature. In addition the melts containing 70 and 75 at% Au were measured at 600°C.

The total structure factors are given for the different melts in Figure 1. These runs were obtained according to the method of cubic spline fit to the measured data in the region $0.2 \leq q \leq 9$ Å^{-1}. Some characteristic data of these functions are given together with the measuring temperature and the linear coefficients of attenuation in Table I.

TABLE I

Au-Cs-melts: Total structure factor data

Cs-concentration [at%]	T [°C]	μ [cm^{-1}]	q_1[a] [Å^{-1}]	q_2[b] [Å^{-1}]	$S(q_1)$
80	420	0.228	1.85	3.87	1.13
75	450	0.277	1.87	3.85	1.18
70	500	0.319	1.90	3.88	1.31
60	600	0.449	1.95	3.83	1.47
55	640	0.546	1.97	3.88	1.46
53	640	0.596	1.99	3.90	1.46
50	640	0.653	2.00	3.90	1.44

[a] q_1, q_2 = position of the first, second main maximum.
[b] $S(q_1)$ = height of the first main maximum.

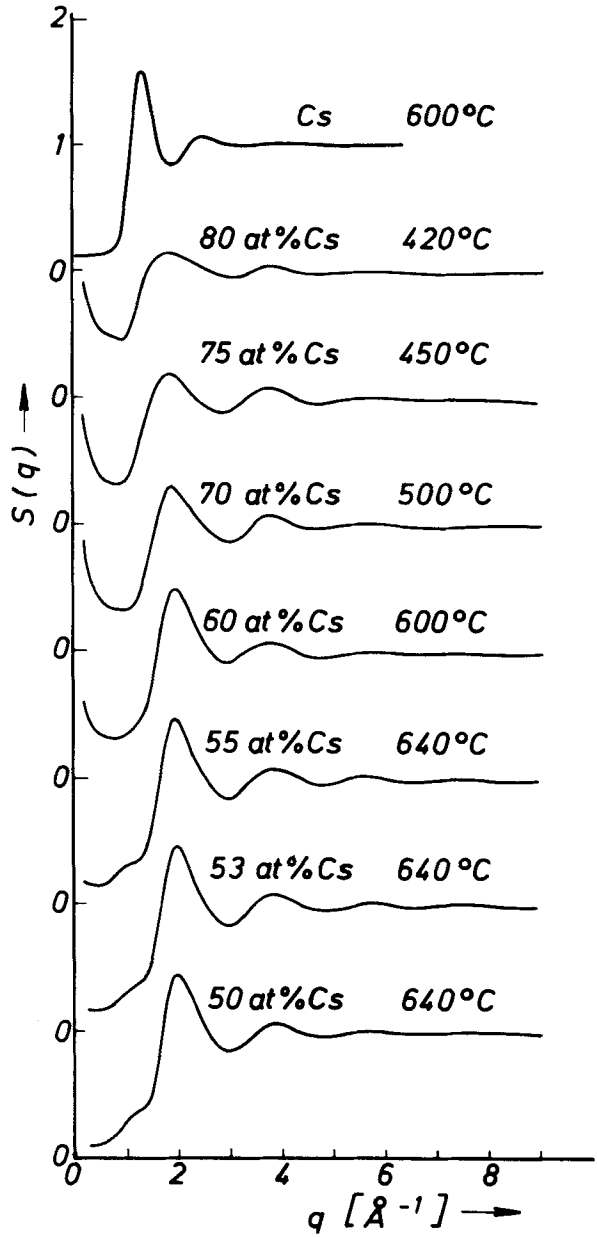

FIGURE 1 Au-Cs melts: Total structure factors.

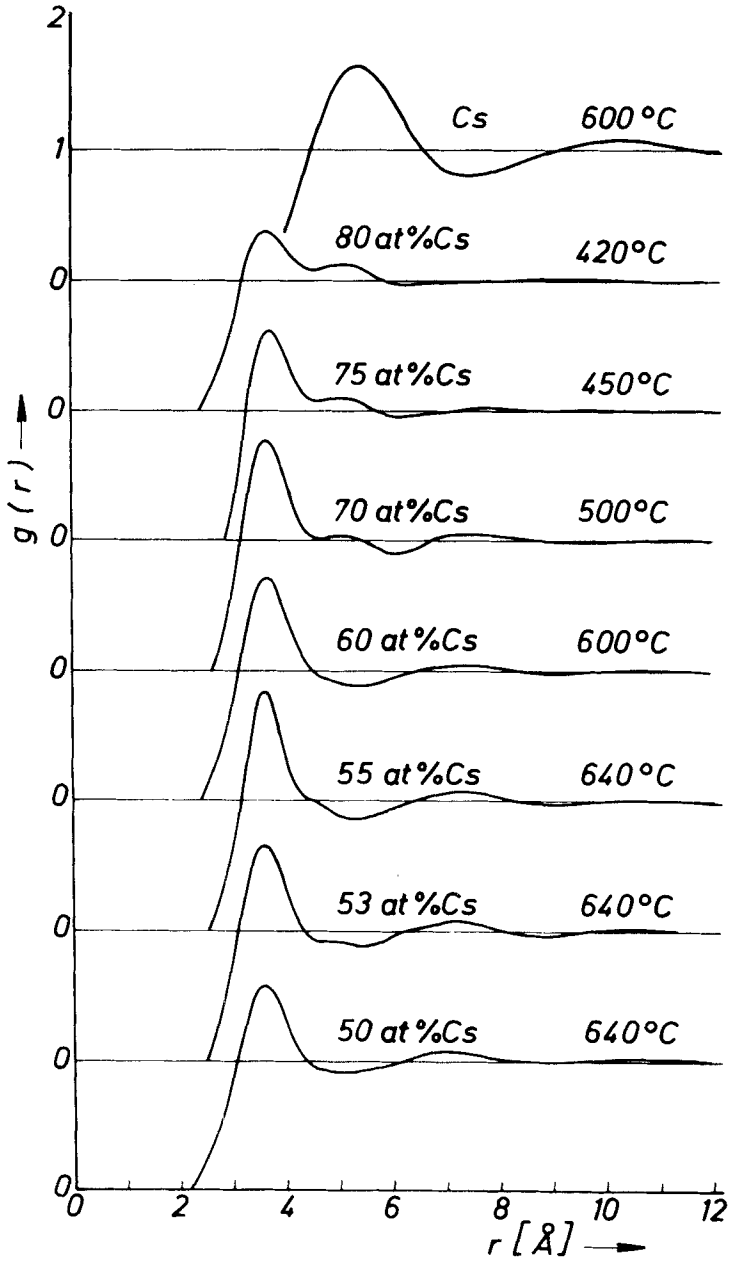

FIGURE 2 Au-Cs melts: Total pair correlation functions.

TABLE II

Au-Cs-melts: Typical data of the total pair correlation functions

Cs-concentration [at%]	Temperature [°C]	r^{I} [Å]	r^{II} [Å]	r^{a} [Å]
80	420	3.63	9.25	5.12
75	450	3.63	7.70	5.10
70	500	3.62	7.35	5.10
60	600	3.60	7.30	—
55	640	3.59	7.28	—
53	640	3.59	7.15	—
50	640	3.58	6.95	—

r^{I}, r^{II} = Radii of the first and second coordination sphere.
r^{a} = Position of the additional maximum between the first and second main maximum.

The total pair correlation functions $g(r)$ are plotted in Figure 2 versus r. The oscillations below $r = 2$ Å caused by the finite integration length are already eliminated and replaced by $g(r) = 0$.

Table II contains the radii r^{I} and r^{II} of the first and second coordination sphere as well as the position r^{a} of the additional maximum which can be observed in Figure 2 for the Cs-rich alloys containing more than 70 at% Cs between the first and second main maximum.

DISCUSSION OF THE RESULTS

From Figure 1 and Table I a shift of the first main maximum of $d\sigma/d\Omega|_{coh}(q)$ to larger q-values due to decreasing Cs-concentration can be deduced. At the same time the height of the main maximum increases. The position of the second main maximum remains almost unchanged. The effect of small angle scattering of the melts with 60 to 80 at% Cs will be treated in Ref. 12. Further addition of Au decreases the height of the structure factor at $q = 0.2$ Å^{-1}. Thus the small angle scattering is only weak for the melts containing 55 and 53 at% Cs and it vanishes completely for the stoichiometric composition. The structure factors of these melts show a premaximum at $q = 1.2$ Å^{-1} which has a maximum height for the concentration of 50 at% Cs.

As far as we know, up to now no melt composed of metallic components was investigated which showed the effect of small angle scattering (which means segregation tendency) as well as the effect of a premaximum (which means a tendency for compound formation).

The atomic distances in Table II show first only a very small concentration dependence of the distance of nearest neighbours in the whole concentration region.

Starting from a specimen containing 50 at% Cs which shows no special features around the first main maximum, alloying of additional Cs causes additional oscillations between the first and second main maximum of the $g(r)$-function. This leads finally to the additional maximum at $r^a = 5.1$ Å which rises for the melts with 70, 75, and 80 at% Cs whereas at the same time the first main maximum decreases. Caused by this additional maximum the calculation of a coordination number for all melts except that with 50 at% Cs becomes too uncertain. If we use only the symmetric part of the first main maximum we obtain $N^I = 8$ atoms for the AuCs-melt containing 50 at% Cs.

It should be mentioned that the total pair correlation functions show special features in the same concentration region, in which the total structure factors show the effect of small angle scattering.

STRUCTURE OF THE AuCs-MELT

The structure factor of the AuCs-melt cannot be described with the hard sphere model given by Ashcroft and Langreth for the statistical distribution of the atoms of both kinds.[13] According to Ref. 14 such deviations from the statistical distribution of the atoms of both kinds should lead to negative deviations from the value for statistical distribution in the run of r^1 and N^1 versus the concentration. For statistical distribution the following equations are valid:[15]

$$r_{st}^I = \frac{\sum_i c_i b_i r_i^I}{\langle b \rangle} \tag{8}$$

$$N_{st}^I = \sum_i c_i N_i^t \tag{9}$$

with

r_i^I = radius of the first coordination sphere of the element i
N_i^I = coordination number of the first coordination sphere of the element i

With the figures from Ref. 8 we obtain

$$r_{st}^I = 3.92 \text{ Å} \quad \text{and} \quad N_{st}^t = 10 \pm 1 \text{ atoms}$$

Since the experimentally obtained figures always were smaller, the AuCs-melt indeed shows compound forming tendency.

a) Radius of the first coordination sphere

As already mentioned in the introduction, the results of the investigations of specific conductivity, electromigration, thermopower and magnetic susceptibility can only be explained by the assumption that the AuCs-

melt consists of Cs^+- and Au^--ions. Therefore a comparison of the structural data of the AuCs-melt with those of molten salts will be performed.

In numerous papers neutron- and X-ray-diffraction-experiments with molten alkali halides were described (see Refs. 16, 17). By the application of the method of isotopic substitution to the neutron diffraction method the partial structure factors could be determined for KCl and CsCl[18] as well as for RbCl.[19] The following facts can be deduced from these papers for ionic melts:

a) The ions are arranged within the melt in such a way, that an ion with positive charge prefers neighbouring ions with negative charge and vice versa.

b) The position of the first maximum in the total pair correlation function can be identified in good approximation with the equilibrium anion-cation distance.

c) The sum of ionic radii according to Pauling[20] is only by 3% larger than the distance of nearest neighbours in the molten state.

If we use the assumption that the observed compound formation in the AuCs-melt corresponds to a charge transfer from Cs to Au and thus to the formation of an ionic compound Cs^+Au^-, a radius for the negative Au-ion can be calculated. In a first approximation we obtain from the radius of the first coordination sphere (3.57 Å) and the Pauling-radius of a Cs-ion[20] (1.67 Å) the radius of the negative Au^--ion as 1.90 Å. This must be compared with $r_{Au}^- = 2.0$ Å which was assumed in Ref. 3 for the theoretical calculation of the magnetic susceptibility of Au-Cs-melts. In addition a comparison will be done with the interatomic distance in the solid state: The AuCs-phase crystallizes in the Cs-Cl-structure and is ionic.[21] The interatomic distance amounts to 3.69 Å and therefore is by 0.12 Å larger than the corresponding distance in the melt. Such a decrease in the interatomic distance was also observed during the melting of alkali halides.[17]

However, the coordination number of molten alkali halides is typically of the order of 6 to 7 (see Refs. 23, 24). The coordination number 8 obtained during the present work for molten AuCs will be discussed in the following section.

b) Coordination number

Abramo *et al.*[22] performed model calculations using the mean spherical model for binary molten salts consisting of hard spheres with different ionic radii. The authors defined a packing density η:

$$\eta = \frac{4\pi}{6} \rho_0[(r^+)^3 + (r^-)^2] \tag{10}$$

and a so-called plasma parameter:

$$\Gamma = \frac{e^2}{2k_B T r^-} \tag{11}$$

with r^+, r^- = ionic radii.

By means of this model the influence of the ratio of radii r^+/r^- on the number of nearest neighbours N^{+-} was investigated. N^{+-} means the number of negative ions around a positive ion. Figure 3 shows the results of these calculations for two different packing densities and $\Gamma = 45.4$. As deduced above, r^+/r^- equals 0.88 for the ionic AuCs-melt. For the plasma parameter we obtain with $r_{Au}^- = 1.9$ Å $\Gamma = 48$. The functions plotted in Figure 3 are Γ-independent in the region $20 < \Gamma < 50$ as shown in Ref. 22.

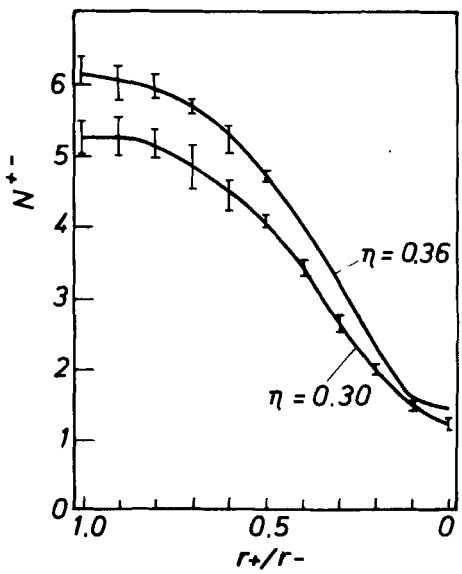

FIGURE 3 Number of nearest neighbours versus r^+/r^- according to Reference 22.

According to Eq. (10) the packing density of the molten compound AuCs amounts to $\eta = 0.53$. Since according to Figure 3 an increase in packing density yields a larger coordination number we can deduce for molten AuCs ($r^+/r^- = 0.88$ N^{+-} in any case to be larger than 6 ions. Taking furthermore into account the uncertainties during the evaluation of the experimental coordination number, we can conclude that the measured coordination number $N^{\text{I}} = 8$ is not in contradiction with the assumption of the AuCs-melt to be similar to a molten salt.

c) Discussion of the premaxium

In this section we will discuss the diffuse maximum on the lower q-side of the first main maximum in the structure factor of molten AuCs. According to Refs. 23, 24 molten salts yield $S_{NC}(q) = 0$. If we assume this also for molten AuCs, from Eq. (1) we obtain:

$$S(q) = S_{NN} + \frac{c_1 c_2 (b_1 - b_2)^2}{\langle b \rangle^2} \left(\frac{S_{CC}}{c_1 c_2} - 1 \right) \tag{12}$$

To evaluate the two partial functions S_{NN} and S_{CC} two experiments would be sufficient. Since no stable isotopes from Au and Cs are known, no further neutron diffraction experiment is possible. An X-ray diffraction experiment cannot be performed at this time since the experimental difficulties are too large. Thus, for the interpretation of the premaximum we assume besides $S_{NC}(q) = 0$ also that it is caused by concentration fluctuations (see, for example, Ref.), i.e. $S_{CC}(q)$.

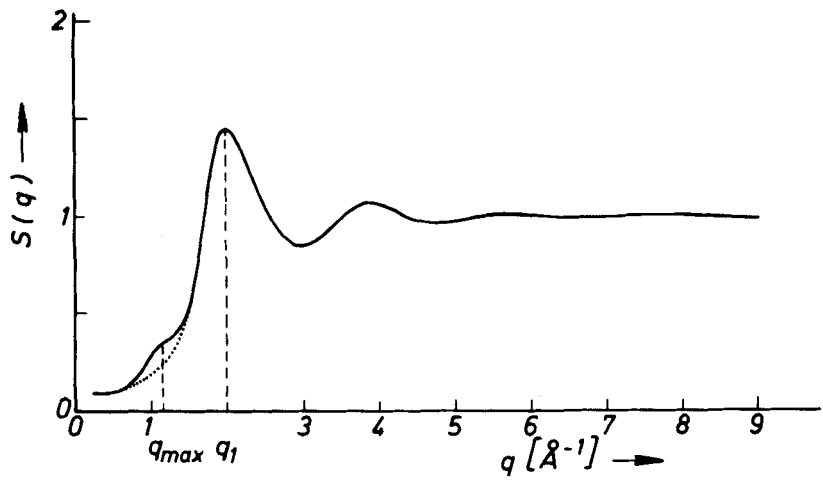

FIGURE 4 Molten AuCs: Total structure factor, ——— Experimental run, ... Interpolated run in the region of the premaximum.

In Figure 4 the $S(q)$ to be expected without premaximum is drawn as dotted lie. According to our assumption this run is determined mainly by $S_{NN}(q)$ for $0.5\,\text{Å}^{-1} \leq q \leq 1.5\,\text{Å}^{-1}$. From Figure 4 we obtain the height of the premaximum $\Delta S = S - S_{NN}$ and from Eq. (12) $S_{CC}(q_{max})/c_1 c_2$ which is tabulated in Table III together with the corresponding figures obtained with different molten salts and semiconductors.

TABLE III

	Molten semiconductors		Molten salts				
	LiPb	Mg_7Bi_3	CsCl	RbCl	KCl	Melt model	AuCs
Ref.	26	25	23	24	23	28	present paper
$S_{CC}(q_{max})/c_1c_2$	1.7	2.7	3.2	3.7	4.8	3.4	4.1
$S_{NN}(q_1)$	2.2	1.76	1.47	1.49	1.33	1.25	1.44
ΔZ	0.8	0.6	2.3	2.2	2.2	—	1.7

[a] $S_{CC}(q_{max})/c_1c_2$: Normalized height of the first maximum in $S_{CC}(q)$ (premaximum) according to Eq. (12).
[b] $S_{NN}(q)$: Height of the first maximum in $S_{NN}(q)$ (main maximum of $S(q)$).
[c] ΔZ: Difference of electronegativities.

Table III furthermore contains the height of the first maximum of $S_{NN}(q)$ which is nearly the same as the height of the first maximum of $S(q)$. Furthermore the difference of electronegativities is tabulated. The comparison of the group of molten salts with that of molten LiPb and molten $Mg_{0.7}Bi_{0.3}$ (for the stoichiometric composition Mg_3Bi_2 no data are available) which both are classified as molten semiconductors in literature shows that $S_{CC}(q_{max})/c_1c_2$ is larger for molten salts and that it decreases with increasing radius of the alkali-ion. From this point of view Mg_3Bi_2 is to be placed just between LiPb and molten salts. This conclusion concerning Mg_3Bi_2 is also valid for $S_{NN}(q_1)$. In this case, however, the figures for molten semiconductors are larger than those for molten salts. Concerning the difference ΔZ of electronegativities, molten AuCs resembles more to molten salts than to molten semiconductors. This feature also is valid for the partial structure factors $S_{CC}(q_{max})/c_1c_2$ and $S_{NN}(q_1)$ which for the AuCs-melt are indeed as typical for salts. Regarding the simplifying assumption which we made and also the large inaccuracy during the separation of the premaximum, the accordance is very good. A further argument for the salt-like structure of molten AuCs can be derived from its ratio $q_{max}/q_1 = 0.6$ which is very similar to the ratio 0.57 typical for ideal ionic melts.[28]

According to measurements of the electrical conductivity with molten AuRb[29] a similarity with molten AuCs can be recognized, too. Since the ionic radii of Cs^+ and Rb^+ are nearly the same and also the differences of the electronegativity between Au and Cs on the one hand and Au and Rb on the other hand are nearly equal, similar structures can be expected for molten AuRb and molten AuCs. Since furthermore the neutron scattering lengths of Rb and Au are equal, a neutron diffraction experiment to be performed with molten AuRb should show no premaximum. This would be an indirect proof for the assumption made in the present paper, namely that the premaximum can be attributed to S_{CC} only.

STRUCTURE OF THE MELTS CONTAINING MORE THAN 50 at% Cs

According to the pair correlation function in Figure 2 the radius of the first coordination sphere of the Cs-rich alloys is nearly the same as for the molten AuCs-compound. From the decreasing height of the first main maximum in $g(r)$ with increasing Cs-content we learn that the probability of the occurrence of this distance in the melt depends on the concentration of Cs and becomes smaller. Parallel to the increasing Cs-content an additional maximum at $r^a = 5.12$ Å is formed which is 0.2 Å smaller than the atomic distance in molten Cs.

Thus we conclude that the Cs-rich melts consist in the average of time of ionic AuCs-regions and of atomic Cs-regions which are microscopically segregated as follows from the evaluation of the small angle scattering experiments (see Ref. 12). In the following we will compare the differential coherent scattering cross sections of Cs-rich melts with cross sections which follow from a model. According to this model, the melt consists of a macroscopically segregated melt of atomic Cs and ionic AuCs.

$$\left.\frac{d\sigma}{d\Omega}\right|_{coh}^{seg} = a_{AuCs}\left.\frac{d\sigma}{d\Omega}\right|_{coh}^{AuCs} + a_{Cs}\left.\frac{d\sigma}{d\Omega}\right|_{coh}^{Cs} \tag{13}$$

The concentrations a_{AuCs} and a_{Cs} are defined as follows:

$$a_{AuCs} = 2c_{Au}$$

$$a_{Cs} = 1 - 2c_{Au}$$

This model calculation is independent of temperature. We introduce into Eq. (13) the differential coherent scattering cross sections of molten AuCs (640°C) and of molten Cs (600°C) and compare the cross section thus obtained in Figure 5 with those obtained experimentally from Au-Cs-melts with 60, 70, and 75 at% Cs (600°C). This model describes the experimental curves for $q > 1$ Å^{-1}, i.e., the discussion is restricted to the high-angle region.

The difference between the distances of nearest neighbours ($r^I_{AuCs} = 3.57$ Å; $r^I_{Cs} = 5.43$ Å) is large. Therefore the segregation model yields a distinct splitting of the main maximum. This splitting becomes enforced with growing Cs-concentration. The experimental curves do not show this feature, whereas the position and breadth of the first main maximum is approached rather good by the model calculations. This means the macroscopic segregation to be replaced by the microscopic segregation in atomic dimensions in the real melt. The existence of "mixed distances" in the regions between the volumes containing Cs-atoms and those containing agglomerates from Cs^+- and Au^--ions yields the smearing out of the splitting.

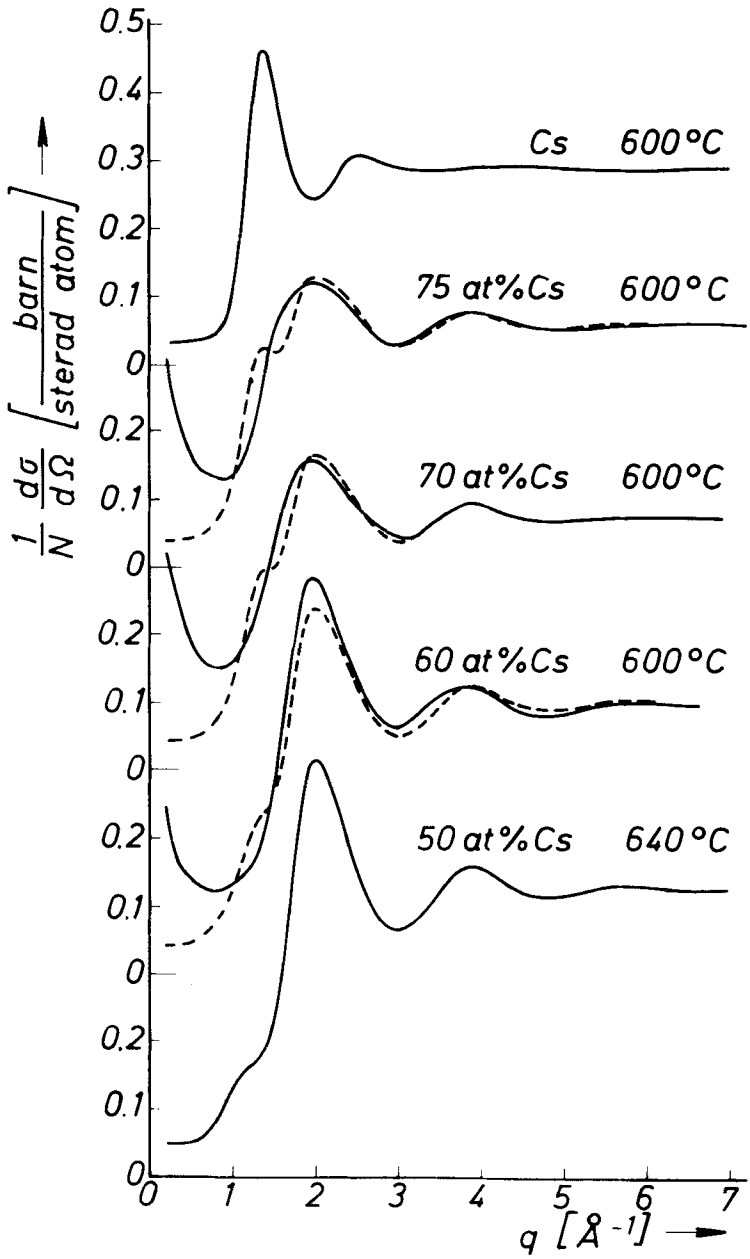

FIGURE 5 AuCs-Cs-melts: Coherent differential scattering cross section per atom, ——— Experimental run, ... Model of total segregation.

With increasing Cs-concentration the high q-side of the first main maximum becomes more flat. This feature is very well reproduced by the model calculation and is due to the influence of the the second maximum in $(1/N)\mathrm{d}\Omega|_{\mathrm{cox}}^{\mathrm{Cs}}$ which is appreciable in this region. The accordance for q larger than 3.0 $\mathrm{Å}^{-1}$ is excellent. From this fact one can conclude, that the run of the curve above $q = 3.0\ \mathrm{A}^{-1}$ is by far determined by

$$\left.\frac{1}{N}\frac{\mathrm{d}\sigma}{\mathrm{d}\Omega}\right|_{\mathrm{coh}}^{\mathrm{AuCs}},$$

since the Cs-curve in this region can be nearly neglected.

Finally it should be pointed out that the existence of two phases with the composition AuCs and Cs can be used in an excellent way to understand the experimental run[1] of the specific electrical conductivity in this concentration region.

SUMMARY

Diffraction experiments with hot neutrons (0.692 Å) were performed with molten Au-Cs-alloys containing 50, 53, 55, 60, 70, 75, and 80 at % Cs, which yielded total structure factors and total pair correlation functions.

The total structure factor obtained experimentally from an AuCs-melt cannot be explained by a statistical model. A further evidence for a nonstatistical structure is formed by the diffuse additional maximum in the lower q-region of the main maximum. The distance of nearest neighbours as well as the number of atoms of the first coordination sphere can be explained by the existence of an ionic AuCs-compound with a radius of Au^- equal to 1.9 Å. The compound formation in the AuCs-melt is based on a charge transfer and thus the additional maximum is determined by concentration fluctuations.

Adding Cs to the AuCs-melt, beside the distance characteristic for AuCs an additional distance can be observed which corresponds to the radius of the first coordination sphere of molten Cs. In addition a model based on macroscopic segregation enforces the assumption of the existence of Cs besides AuCs. By means of this model the experimental run of the coherent differential scattering cross section per atom within the melts containing 60, 70, and 75 at % Cs can be well explained for $q > 1\ \mathrm{Å}^{-1}$.

References (Part II)

1. R. W. Schmutzler, H. Hoshino, R. Fischer, and F. Hensel, *Ber. Bunsenges. Physik. Chem.*, **80**, 107 (1976).
2. K. D. Krüger and R. W. Schmutzler, *Ber. Bunsenges. Physik. Chem.*, **80**, 816 (1976).
3. W. Freyland and G. Steinleitner, *Ber. Bunsenges. Physik. Chem.*, **80**, 810 (1976).

4. F. Hensel, *Ber. Bunsenges. Physik. Chem.*, **80**, 786 (1976).
5. J. P. Suchet, *Chemical Physics of Semiconductors*, D. van Nostrand Comp., London (1965).
6. T. E. Faber and J. M. Ziman, *Phil. Mag.*, **11**, 153 (1965).
7. A. B. Bhatia and D. E. Thornton, *Phys. Rev.*, **B2**, 3004 (1970).
8. W. Martin, W. Freyland, P. Lamparter, and Steeb, *J. Phys. Chem. Liq.* **10**, 49 (1980) (I).
9. G. H. Vineyard, *Phys. Rev.*, **96**, 93 (1954).
10. V. F. Sears, *Adv. in Phys.*, **24**, 1 (1975).
11. R. P. Elliot, *Constitution of Binary Alloys, First Supplement*, McGraw-Hill Book Co., New York (1965).
12. W. Martin, W. Freyland, P. Lamparter, and S. Steeb, *J. Phys. Chem. Liq.*, **10**, 77 (1980) (III).
13. N. W. Ashcroft and D. C. Langreth, *Phys. Rev.*, **156**, 685 (1967).
14. S. Steeb, Habilitationsschrift, Universität Stuttgart (1969).
15. P. Lamparter, Dissertation, Universität Stuttgart (1976).
16. J. Zarzycki, *J. Phys. Rad. Suppl.*, **4**, 13A, (1958).
17. H. A. Levy, P. A. Agron, M. A. Bredig, and M. D. Danford, *Ann. N.Y. Acad. Sci.*, **79**, 762 (1960).
18. J. Y. Derrien and J. Dupuy, *J. Phys. (Paris)*, **36**, 191 (1975).
19. E. W. J. Mitchell, P. F. J. Poncet, and R. J. Stewart, *Phil. Mag.*, **34**, 721 (1976).
20. L. Pauling, *Nature of the Chemical Bond*, Cornell Univ. Press, Ithaca, New York (1960).
21. K. H. Jack, H. M. Wachtel, *Proc. Roy. Soc.*, **A239**, 49 (1957).
22. M. C. Abramo, C. Caccomo, G. Pizzimenti, M. Parrinello, and M. P. Tosi, *J. Phys. C.*, **9**, *L593* (1976).
23. J. Y. Derrien, Thése, Université Lyon (1976).
24. P. F. J. Poncet, Thesis, University of Reading, UK (1976).
25. A. Boos, S. Steeb, *Phys. Lett.*, **63A**, 33 (1977).
26. These data are based on measurements by H. Ruppersberg, H. Egger, *J. Chem. Phys.*, **63**, 4095 (1975) and were taken from J. Blétry, *Z. Naturforschung*, **33a**, 327 (1978).
27. L. S. Darken, *Trans. Aime*, **239**, 80 (1967).
28. J. P. Hansen, I. R. McDonald, *Phys. Rev.*, **11**, 2111 (1975).
29. N. Nicoloso, R. W. Schmutzler, and F. Hensel, *Ber. Bunsenges. Physik. Chem.*, **82**, 621 (1978).